Analog gravity by an optical vortex: Resonance enhancement of Hawking radiation

Marco Ornigotti,[1,*] Shimshon Bar-Ad,[2] Alexander Szameit,[1] and Victor Fleurov[2]
[1]*Institut für Physik, Universität Rostock, Albert-Einstein-Straße 23, 18059 Rostock, Germany*
[2]*Raymond and Beverly Sackler Faculty of Exact Sciences, School of Physics and Astronomy, Tel-Aviv University, Tel-Aviv 69978, Israel*

(Received 25 April 2017; revised manuscript received 28 December 2017; published 17 January 2018)

Propagation of coherent light in a Kerr nonlinear medium can be mapped onto a flow of an equivalent fluid. Here we use this mapping to model the conditions in the vicinity of a rotating black hole as a Laguerre–Gauss vortex beam. We describe weak fluctuations of the phase and amplitude of the electric field by wave equations in curved space, with a metric that is similar to the Kerr metric. We find the positions of event horizons and ergoregion boundaries, and the conditions for the onset of superradiance, which are simultaneously the conditions for a resonance in the analog Hawking radiation. The resonance strongly enhances the otherwise exponentially weak Hawking radiation at certain frequencies and makes its experimental observation feasible.

DOI: 10.1103/PhysRevA.97.013823

I. INTRODUCTION

Analog gravity is a research field aimed at creating table-top experimental systems which model processes generally described within the framework of general relativity (GR). It is one of the directions of a broader field aiming at merging quantum mechanics and general relativity [1]. The research field of analog gravity essentially originated from the seminal paper by Unruh in 1981 [2], where the analog of Hawking radiation [3,4] in a transonically accelerating inviscid barotropic fluid in a linear geometry was discussed. In his work, Unruh showed that the accelerating flow in linear geometry creates a background, which mimics curved space with the Schwarzschild metric, and that weak fluctuations with respect to such background are described by the corresponding Klein–Gordon equation (see Ref. [5] for detailed explanations). More recently, several different physical systems were theoretically proposed, in which the necessary conditions for the onset of a Schwarzschild metric can occur, such as ^{3}He [6], solid-state systems [7], one-dimensional Fermi liquids [8], Bose–Einstein condensates (BECs) [9–11], superconducting devices [12], and optical fluids [13–17], to name a few. Moreover, "horizon physics" for surface waves in a water channel has also been investigated [18–22] and, recently, the possibility for a "magnonic" black hole has been discussed as well [23,24]. Parallel to theoretical proposals, significant progress in the experimental realization of analog gravity systems has also been made, like the observation of a white-hole horizon in optical fibers [25,26], or the realization of a black-hole horizon in BECs by Steinhauer and coworkers [27], who also reported on evidence of Hawking radiation in such a system [28]. Moreover, stimulated amplification of Hawking radiation [29], in accordance with the predictions of Ref. [30], has also been reported.

In nearly all aforementioned works, however, the background-induced metric is always the same; namely, the Schwarzschild metric, which describes the spacetime in the vicinity of an ordinary, nonrotating, back hole. In GR, on the other side, there are different metrics that admit black holes as a solution. It would therefore be very interesting to construct analog models for other types of black-hole metrics and to study the effects of these alternative geometries on the process of Hawking radiation. For example, it would be of particular interest to realize an analog of a rotating black hole. In this case, the relevant metric would be the Kerr metric [5], rather than the standard Schwarzschild metric. Moreover, in such a geometry one would be able to observe not only Hawking radiation, but also superradiance (SR), i.e., the conditions when an incident wave may be amplified by the rotating black hole itself, so that the reflected wave is stronger than the incident one. A vortex in a fluid, in particular, is an exciting possibility for studying the dynamics of fields in the vicinity of rotating black holes. In such a system, the vortex induces a Kerr-type metric [5] and essentially plays the role of the rotating black hole. In particular the SR effect for the case of vortices in shallow water [20], as well as for BEC [31], has been predicted. Very recently, moreover, SR from a vortex in shallow water has also been reported experimentally [32].

Water waves and atomic systems, however, are not the only media, in which vortices appear. Vortices, in fact, are also known to occur in optics. As shown by the pioneering works of Berry and Nye in 1974 [33] and Allen and Woerdman in 1992 [34], optical fields that carry phase singularities, e.g., Laguerre–Gaussian beams, have transverse intensity profiles with all the characteristics of a vortex [35]. Moreover, it is also well known that coherent light propagation in defocusing nonlinear Kerr media [36] is analogous to the flow of a fluid, and even a superfluid, by virtue of the so-called hydrodynamic approach to Maxwell's equations. This approach was instrumental for investigating dispersive shock waves [37–39] and tunneling processes [40], and its application to the field of analog gravity was discussed theoretically and experimentally in Refs. [13–15,41,42]. The fluctuations in such equivalent-photon fluids are predicted to be of the Bogoliubov type [16,43–46], and recent measurements of their dispersion

*marco.ornigotti@uni-rostock.de

relation [47] support this prediction. It is important to emphasize that such an optical system is effectively isolated from the thermal bath of the medium due to enormous difference of the light velocity and that of the thermal fluctuations. So the criterion of Ref. [48], which yields the limiting temperature in BEC above which entanglement is destroyed, is not applicable here.

Yet, despite a considerable volume of work dealing with the hydrodynamic approach to Maxwell's equations, to the best of our knowledge a comprehensive theory of Hawking radiation from a black hole event horizon in a vortex background has not been studied. The only exception, however, is represented by the works of Marino and coworkers [13,14]. In these works, the hydrodynamic approach is used to describe the propagation of light in an optical cavity filled by a defocusing medium. In particular, they carefully show how an analog of a rotating black hole in such a system can be realized by suitably controlling the properties of the vortex state sustained by the cavity. However, the principal attention of these works is concentrated on the study of SR and although the possibility of using this system to study Hawking radiation is envisaged, this phenomenon is not studied in detail.

Hence, we devote this paper to this open question. In particular, we consider Laguerre–Gaussian beam propagating in a defocusing Kerr nonlinear medium and study the dynamics of fluctuations of the electromagnetic field on such a vortex background, leading to Hawking radiation and SR. We discuss the strong connection between these two phenomena and show that the conditions for the onset of SR coincide with resonance enhancement of certain frequencies of Hawking radiation.

This paper is organized as follows: in Sec. II we shortly review the hydrodynamic formulation of the nonlinear Schrödinger equation in nonlinear optical media and cast the problem for analysis; namely, the field fluctuations in a nonstationary vortex background with a radial flow. In Sec. III we discuss how to obtain the nonvanishing radial flow that is essential for the appearance of an event horizon in the vortex background. Section IV is then devoted to analyzing the induced "spacetime" geometry, including the positions of event horizons and ergoregions. Section V is then dedicated to calculation of the Hawking temperature as a function of the background vorticity, and to the discussion of the spectral density of Hawking radiation, with a particular emphasis on the occurrence of its resonant enhancement, which is essentially due to the background vorticity. Finally, conclusions are drawn in Sec. VI. Moreover, the occurrence of SR is investigated in detail in Appendix B.

II. FIELD FLUCTUATIONS IN A VORTEX BACKGROUND WITH RADIAL FLOW

A. Hydrodynamic formulation of nonlinear Schrödinger equation

The propagation of electromagnetic waves in Kerr nonlinear media can be described, under the paraxial and the slowly varying envelope (SVEA) approximations, by the following nonlinear Schrödinger equation [49]:

$$i\frac{\partial A}{\partial z} = -\frac{1}{2\beta_0}\nabla_\perp^2 A + g|A|^2 A, \tag{1}$$

where the propagation distance z plays the role of time, $\mathbf{R} = \{r,\phi\}$, $A \equiv A(\mathbf{R},z)$ is the slowly varying amplitude of the electric field propagating in the medium along the z direction, $\nabla_\perp^2$ is the transverse Laplace operator with respect to the variables x and y, or r and ϕ in polar coordinates, $\beta_0 = \omega_0 n_0/c = k_0 n_0$ is the wave vector of the field in the medium, and ω_0 is the laser frequency. The parameter $g = 2\beta_0 n_2/n_0$ describes the strength of the nonlinear interaction of the laser EM field with the medium, with n_2 being the Kerr nonlinear refractive index, i.e., $n(A) = n_0 + n_2|A|^2$. Applying the Madelung transformation [50,51] $A(\mathbf{R},z) = f(\mathbf{R},z)\exp[-i\varphi(\mathbf{R},z)]$, we obtain the following coupled differential equations:

$$\frac{\partial \rho}{\partial z} + \nabla_\perp \cdot (\rho \mathbf{v}) = 0, \tag{2a}$$

$$\frac{\partial \mathbf{v}}{\partial z} + \frac{1}{2}\nabla_\perp(\mathbf{v}\cdot\mathbf{v}) = -\frac{1}{\beta_0}\nabla\left[-\frac{1}{2\beta_0}\frac{\nabla_\perp^2 f}{f} + g\rho\right], \tag{2b}$$

for the density $\rho(\mathbf{R},z) = f^2(\mathbf{R},z)$ and the velocity $\mathbf{v} = -(1/\beta_0)\nabla\varphi(\mathbf{R},z)$. The first term on the right-hand side of Eq. (2b) is the so-called quantum potential, which accounts for dispersion in the medium. Equations (2) can be seen as the continuity and Euler equations for a fluid characterized by density ρ and velocity $\mathbf{v}$. In this form, light dynamics in a Kerr nonlinear medium is similar to the dynamics of a compressible fluid. Usually, the next step would be to consider small fluctuations $A = \Phi_0 + \psi$ around a z-stationary solution Φ_0, i.e., the function Φ_0 z dependence is only in the factor $e^{i\mu z}$. However, this assumption is not only unnecessary but also undesirable, since creation of a z-stationary flow is unrealistic for flow fields that involve radial velocities (radial flow appears only if the beam profile varies with z). We therefore assume that the z-dependent function $\Phi_0 = f_0\exp(-i\varphi_0)$, and the functions $\rho_0(\mathbf{R},z)$ and $\mathbf{v}_0(\mathbf{R},z)$, solve Eqs. (2) and write the corresponding density and velocity fluctuations in the form $\delta\rho(\mathbf{R},z) = \rho_0(\mathbf{R},z)\chi(\mathbf{R},z)$ and $\delta\mathbf{v}(\mathbf{R},z) = -(1/\beta_0)\nabla\xi(\mathbf{R},z)$. Then, Eqs. (2) can be linearized and written as follows:

$$\hat{\mathcal{D}}\chi - \frac{1}{\beta_0\rho_0}\nabla_\perp(\rho_0\nabla_\perp\xi) = 0, \tag{3a}$$

$$\hat{\mathcal{D}}\xi + \frac{1}{4\beta_0\rho_0}\nabla_\perp(\rho_0\nabla_\perp\chi) - g\rho_0\chi = 0, \tag{3b}$$

where $\hat{\mathcal{D}} = \partial_z + \mathbf{v}_0\cdot\nabla_\perp$. The above set of equations is equivalent to the one obtained for fluctuations on a z-stationary background [52]. However, in this case, the density ρ_0 and velocity v_0 are weakly z dependent.

B. Fluctuations in a vortex background

If we neglect the quantum potential in Eq. (3b), solve it with respect to χ, and substitute into Eq. (3a), we get the Klein–Gordon equation

$$\frac{1}{\sqrt{\det(-g_{\mu\nu})}}\partial_\mu\left(g^{\mu\nu}\sqrt{\det(-g_{\mu\nu})}\,\partial_\nu\xi\right) = 0 \tag{4}$$

for the phase fluctuation ξ in the curved space determined by the background flow of the z-nonstationary solution $\Phi_0(\mathbf{R},z)$.

The contravariant metric in polar coordinates is then

$$g^{\mu\nu} = \frac{1}{s}\begin{pmatrix} 1 & v_r & \frac{v_\phi}{r} & 0 \\ v_r & v_r^2 - s^2 & \frac{v_r v_\phi}{r} & 0 \\ \frac{v_\phi}{r} & \frac{v_r v_\phi}{r} & \frac{\left(v_\phi^2 - s^2\right)}{r^2} & 0 \\ 0 & 0 & 0 & -s^2 \end{pmatrix}, \tag{5}$$

where we assume that the background flow velocity $\mathbf{v}_0 = v_r\hat{\mathbf{r}} + v_\phi\hat{\boldsymbol{\phi}}$ contains both a rotational and an azimuthal component. The quantity s is the sound velocity of the background flow, defined as follows:

$$\beta_0 s^2 = g f_0^2. \tag{6}$$

Although we consider t-stationary solutions, a 4×4 metric is used as a matter of convenience. The fourth coordinate (measured in properly chosen units) is redundant and can be omitted whenever necessary.

By inverting Eq. (5) we find the covariant metric describing the background; namely,

$$g_{\mu\nu} = \frac{1}{s}\begin{pmatrix} s^2 - v_0^2 & v_r & r v_\phi & 0 \\ v_r & -1 & 0 & 0 \\ r v_\phi & 0 & -r^2 & 0 \\ 0 & 0 & 0 & -1 \end{pmatrix}, \tag{7}$$

where $v_0^2 = v_r^2 + v_\phi^2$. In the general case, Eq. (7) represents a Kerr-type metric and therefore delineates two special contours corresponding to the boundary of the ergoregion and the event horizon of a rotating black hole [53]. To let them explicitly appear in the above metric, we first introduce the generalized tortoise coordinates

$$\begin{aligned} d\tilde{z} &= dz + \frac{v_r}{s^2 - v_r^2}dr, \\ d\tilde{r} &= dr, \\ d\tilde{\phi} &= \frac{v_r v_\phi}{r\left(s^2 - v_r^2\right)}dr + d\phi, \end{aligned} \tag{8}$$

such that the interval $d\sigma^2 = g_{\mu\nu}dx^\mu dx^\nu$ becomes

$$d\sigma^2 = \frac{1}{s}\left[\left(s^2 - v_0^2\right)d\tilde{z}^2 - \frac{s^2}{s^2 - v_r^2}d\tilde{r}^2 - r^2 d\tilde{\phi}^2 + 2r v_{\tilde{\phi}} d\tilde{z} d\tilde{\phi}\right]. \tag{9}$$

The radius r_e of the ergoregion is then found from the condition $g_{zz} = 0$, i.e., $v_0^2(r_e) = s^2(r_e)$, whereas the radius r_h of the event horizon corresponds to the point where g_{rr} diverges, i.e., $v_r^2(r_h) = s^2(r_h)$.

For the case of a background whose z-stationary solution $\Phi(\mathbf{R})$ is a vortex of charge n, it follows directly from Eqs. (2) that $\mathbf{v}_0 = v_\phi\hat{\boldsymbol{\phi}} = n/(\beta_0 r)\hat{\boldsymbol{\phi}}$, i.e., there is no radial flow, and, therefore, $v_r = 0$ [51,54]. Substituting this result into Eq. (7) we see that the metric for a pure z-stationary vortex background contains only one singular point, corresponding to the ergoregion.

The dynamics of fluctuations in a vortex background therefore always admit SR, as the ergoregion, according to Eq. (7), is always well defined. This effect was considered for several model systems [31,55,56]. However, the lack of radial flow, i.e., a radial component of the velocity $\mathbf{v}_0$ of the vortex, and the consequent absence of an event horizon, does not allow analysis of the effect of the background vorticity on the Hawking process at the event horizon of a rotating black hole. Introducing radial flow requires consideration of a z-nonstationary vortex background, as discussed in detail in the following section.

III. RADIAL FLOW ON A VORTEX BACKGROUND

The absence of a radial component of the velocity flow $\mathbf{v}_0$ in a z-stationary vortex background is essentially due to Eq. (2a). In fact, for any z-stationary solution $\Phi_0(\mathbf{R})$ of Eq. (1), Eq. (2a) implies that $\boldsymbol{\nabla}_\perp \cdot (\rho_0 \mathbf{v}_0) = 0$. This condition leads immediately to $v_r = 0$. The metric for a pure z-stationary vortex background contains only two singular points, which correspond to two ergoregions. In such a metric, therefore, no event horizon appears. Short of introducing source or sink, we now have to look for weakly z-dependent solutions $\Phi(\mathbf{R},z)$ of Eq. (1).

For the case of an optical beam propagating in a defocusing Kerr medium, we can (at least to the first order in z) assume that the solution to Eq. (1) can be sought in the form of an adiabatically slowly varying paraxial vortex beam, e.g., a Laguerre–Gaussian beam. Although this is rigorously true only for the linear case (i.e., $g = 0$), we can assume that the effect of the defocusing nonlinearity is only to introduce a nonlinear phase shift that does not drastically affect the form of the solution, at least to the first perturbation order.

With this in mind, let us assume that the density and velocity of the quasistationary solution $\Phi(\mathbf{R},z)$ of Eq. (1) can be written as

$$\rho(r,z) = f_0^2(r,z) = I\,P(r,z), \tag{10a}$$

$$\mathbf{v}(r,z) = -\frac{1}{\beta_0}\boldsymbol{\nabla}_\perp\varphi_0(r,z) = \frac{r}{R(z)}\hat{\mathbf{r}} - \frac{n}{\beta_0 r}\hat{\boldsymbol{\phi}}, \tag{10b}$$

where I is the total intensity of the laser beam and

$$P(r,z) = \frac{2}{\pi|n|!w^2(z)}\left(\frac{2r^2}{w^2(z)}\right)^{|n|}e^{-2r^2/w^2(z)} \tag{11}$$

is the normalized intensity profile of a Laguerre–Gaussian beam with

$$w^2(z) = w_0^2\left[1 + \left(\frac{z}{z_R}\right)^2\right], \tag{12}$$

$$\frac{1}{R(z)} = \frac{z}{z^2 + z_R^2} \tag{13}$$

being its z-dependent width and wavefront curvature, respectively. Moreover, $z_R = \beta_0 w_0^2/2$ is the Rayleigh range. As can be seen from Eq. (10b), the radial part of the velocity is related to the wavefront curvature of the beam. Note that, at the beam waist $z = 0$, the wavefront is plane and the radial velocity is zero. Rather than positioning the experimental apparatus far away from the beam waist, where $R(z) \approx z$, we choose to position a defocusing lens with focal length $-f$ at the waist, a short distance z before the input plane of the nonlinear medium, so that the phase front of the beam is no longer planar, resulting in a radial velocity that monotonically increases (from zero on

axis) along the radial coordinate. Following standard Gaussian optics [57] (see Appendix A), the intensity and velocity profiles of the field at the input plane of the nonlinear medium are given, in the limit of small z, by

$$P(r,z) = P_0(r)[1 + P_1(r)z], \tag{14a}$$

$$\mathbf{v}(r,z) = \frac{r}{f}\hat{\mathbf{r}} - \frac{n}{\beta_0 r}\hat{\boldsymbol{\phi}} + O(z), \tag{14b}$$

where

$$P_0(r) = \frac{2}{\pi |n|! w_0^2}\left(\frac{2r^2}{w_0^2}\right)^{|n|} e^{-2r^2/w_0^2}, \tag{15}$$

$$P_1(r) = \frac{2}{f w_0^2}\left[2r^2 - (|n|+1)w_0^2\right]. \tag{16}$$

It is not difficult to show that these density and velocity fields satisfy both the continuity and the Euler equations, up to the order $O(z/f)$. Crucially, the background velocity $\mathbf{v}_0$ now has a radial component: $v_r = r/f$.

As mentioned before, the defocusing nonlinearity adds a nonlinear phase, which essentially acts as a nonlinear defocusing lens [49]. The above equations can be corrected to account for this effect by simply setting $1/f = 1/f_L + 1/f_{NL}$. In this case, f_L accounts for the linear radial flow induced by the lens at the beam waist, while f_{NL} is the focal length of the equivalent defocusing lens generated by the nonlinear defocusing. Ultimately, f_{NL} is related to the nonlinear length of the Kerr medium [49] and accounts for a nonlinear correction to the radial flow.

This very simple experimental configuration allows us to fully explore the effects of vorticity, not only in terms of SR scattering from the ergoregion, as in Refs. [31,55,56], but rather in terms of the dynamics of fluctuations in the vicinity of the event horizon of the vortex background. In what follows, we will use this model to study the effect of the background vorticity on both Hawking radiation and SR.

IV. INDUCED SPACETIME GEOMETRY

A. Event horizon

Our first step is to find the positions of the event horizon and ergoregion and to explore the global geometry described by the vortex background. According to Sec. II, the position of the event horizon is determined by the equation $s^2(r) = v_r^2(r)$; namely,

$$\frac{gI}{\beta_0}P(r) = \frac{r^2}{f^2}. \tag{17}$$

A graphical solution of this equation is shown in Fig. 1. Depending on the values of the parameters, it may have no solution (upper, green curve), one solution (middle, blue curve) or two solutions (lower, red curve). In the case of a single solution, the relation

$$\frac{gI}{\beta_0}\frac{dP(r)}{dr} = \frac{2r}{f^2}, \tag{18}$$

must also hold, and thus the solution in this case is

$$r_c = \sqrt{\frac{n-1}{2}}\,w_0. \tag{19}$$

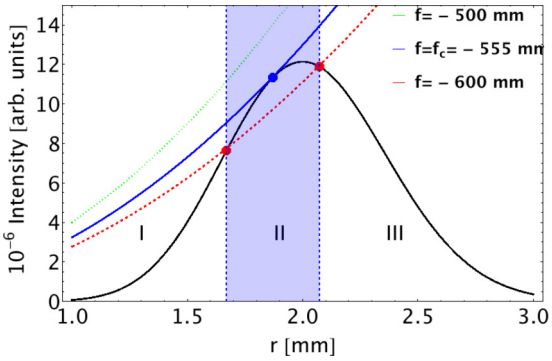

FIG. 1. Graphical solution of equation (17). The bell-shaped curve (in black) represents the Laguerre–Gauss profile of the laser beam, while the three colored curves (dotted green, solid blue, and dashed red) represent the squared radial velocity $v_r^2(r)$ for three different values of the focal length f, corresponding to $f < f_c$, $f = f_c$, and $f > f_c$, respectively. For $f = -500$ mm (upper, dotted, green curve) there are no solutions. For $f_c = -555$ mm (middle, solid, blue curve) there is one solution. For $f = -600$ mm (lower, dashed, red curve) there are two solutions. In the latter case, two event horizons appear, thus introducing a subsonic (region II, shaded in blue in the figure) and a supersonic (regions I and III) region for the flow. The radial intensity profile of the vortex, with vorticity $n = 8$, corresponds to $I = 2$ W, $g = 5.5\times10^{-4}$ m/W, $w_0 = 1$ mm, and $\beta_0 = (2\pi/7.80)\times10^7$ m^{-1}. These parameters allow a broad range of frequencies to satisfy the requirement $L^{-1} < \nu < l_n^{-1}$, where L is the length of propagation in the nonlinear medium, and l_n is the nonlinearity length defined in Eq. (32).

Obviously, Eqs. (17) and (18) admit no solution for $n = 0$, while for $n = 1$ we obtain $r_c = 0$. In general, however, there can only be one nonzero solution, depending on the parameters (e.g., the focal length f).

Two nonzero solutions appear only when $n > 1$ and $|f| < |f_c|$, where the critical value f_c/w_0 depends on the vorticity n. For sufficiently small $\delta f = f - f_c$, the two solutions are slightly below and slightly above r_c:

$$r_{h\pm} = r_c \pm w_0\sqrt{\frac{\delta f}{2f_c}}.$$

For larger δf, the outer horizon r_{h+} falls outside the maximum of the Laguerre–Gauss beam profile (see, for example, the red curve in Fig. 1).

B. Ergoregion

The other singular point appearing in the metric $g_{\mu\nu}$ given by Eq. (9) gives the position of the ergoregion, i.e., the value $r = r_e$ where the total velocity of the fluid equals the background sound velocity, namely $s^2(r) = v_0^2(r)$. For the case of an optical vortex beam propagating in a nonlinear medium, we get

$$\frac{gI}{\beta_0}P(r) = \frac{r^2}{f^2} + \frac{n^2}{\beta_0^2 r^2}. \tag{20}$$

A typical graphical solution is shown in Fig. 2 (lower, blue line), together with the corresponding solution of Eq. (17) (upper, red line). As can be seen from Fig. 2, we obtain two ergoregions: the outer ergoregion r_{e+}, which corresponds to the

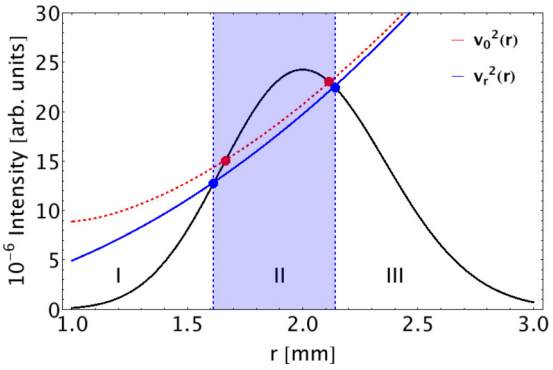

FIG. 2. Graphical solution of Eq. (20). The bell-shaped curve (in black) represents the Laguerre–Gauss profile of the laser beam. The dashed red (upper) curve represents the squared total velocity $v_0^2(r)$ and defines the position of the inner (r_{e-}) and outer (r_{e+}) ergoregions. The solid blue (lower) curve corresponds to the squared radial velocity $v_r^2(r)$ and defines the position of the inner (r_{h-}) and outer (r_{h+}) horizons. There are two ergoregions, one lying between r_{h-} and r_{e-}, and the other lying between r_{e+} and r_{h+}. The parameters used here are the same as in Fig. 1, except for $\beta_0 = (\pi/7.80)\times 10^7$ m^{-1} and $f = -450$ mm. The flow in regions I and III is supersonic, whereas in region II it is subsonic.

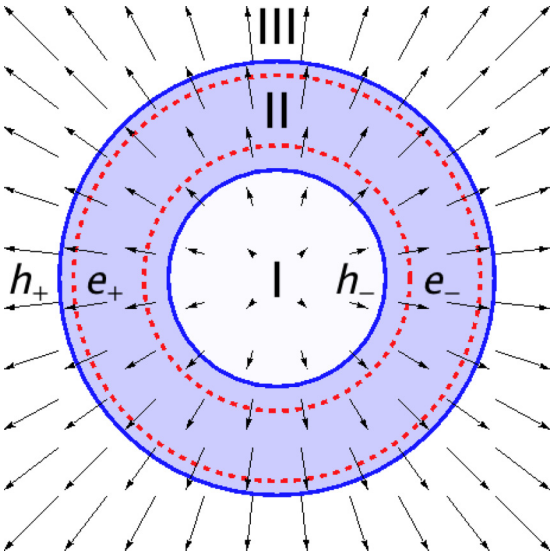

FIG. 3. A schematic depiction of the flow structure of a vortex. Two solid blue circles represent the outer ($h+$) and inner ($h-$) event horizons, separating the supersonic regions I and III from the subsonic region II (shaded blue area). Two dashed red circles show the borders of the outer ($e+$) and inner ($e-$) ergoregions. The arrows show the radial component of the outgoing flow.

outer horizon r_{h+} (close to the border between regions II and III in Fig. 2), and the inner ergoregion r_{e-}, which corresponds to the inner horizon r_{h-} (close to the border between regions I and II in Fig. 2). In both cases, moreover, both ergoregions are inside the subsonic region (shaded blue area, in Fig. 2).

C. Vortex geometry

The resulting two-dimensional (2D) geometry of the background, including the positions of the ergoregions and the event horizons, is depicted in Fig. 3. The inner (h_-) and outer (h_+) horizons are depicted by solid circles, separating three regions: I and III are supersonic regions, while II is subsonic and sandwiched between them (shaded blue area in Fig. 3). It is important to notice that, for the case of a black horizon, the radial component of the flow is directed towards the horizon in the subsonic region, crosses the horizon, and enters the supersonic region. In a white horizon, on the other hand, the direction of the radial flow is from the supersonic to subsonic region. The direction of the azimuthal component of the velocity plays no role in this case. Therefore, in the case of the outgoing flow considered here, the outer horizon h_+ is black, whereas the inner horizon h_- is white. In the case of ingoing flow, the roles of h_+ and h_- are reversed. The two ergoregions e_+ and e_- (dashed circles in Fig. 3) are located inside the subsonic region.

This constitutes a significant difference with respect to the Kerr or Kerr–Newman geometry typical of rotating black holes. Although the latter also has outer and inner horizons, the arrangement of areas of sub- and superluminal escape velocities is the opposite of the one shown here, the ergoregions are positioned differently, and there is no turnaround radius in the optical system [53]. This geometry, moreover, differs from the one presented in Refs. [13,14], where only one event horizon is considered and the radial flow is directed towards the center of the vortex, instead of away from it, as in our case.

V. HAWKING RADIATION WITH VORTEX BACKGROUND

Now we are in a position to analyze the properties of fluctuations near the event horizon. Our approach follows essentially the one used in Refs. [52,58], with some modifications in order to take into account the z dependence of the beam profile and the curvature of the horizon. To begin with, let us introduce the new variables $x_\pm = r - r_{h\pm}$, such that $\partial_r = \partial_x$. Here and below, if not specified otherwise we omit the $\pm$ sign, for the sake of clarity. With this definition, the sound velocity and the radial velocity in the vicinity of the horizons can be written as $s_h^2(x) = s_h^2(1 - \alpha_s x)$ and $v_r(x) = s_h(1 + \alpha_r x)$, respectively. Substituting this into Eqs. (2), the following conditions must hold in the leading order in z:

$$\frac{1}{\rho}\frac{\partial \rho}{\partial z} = -s_h\left(\alpha_r - \alpha_s + \frac{1}{r_h}\right), \tag{21}$$

$$\frac{\partial v}{\partial z} = -s_h^2(\alpha_r - \alpha_s), \tag{22}$$

where s_h is the sound velocity at the horizon and r_h is the position of the horizon. The first condition follows from the continuity equation [Eq. (2a)], while the second follows from the Euler equation [Eq. (2b)]. In the case of the Laguerre–Gaussian beam, we have $s_h = r_h/f$, $\alpha_r = 1/r_h$ and

$$\alpha_s = -\frac{2|n|}{r_h} + \frac{4r_h}{w_0^2}. \tag{23}$$

Then using Eqs. (21) and (22) for the case of a Laguerre–Gauss beam gives

$$s_h(\alpha_r - \alpha_s + 1/r_h) = -P_1(r = r_h). \tag{24}$$

The validity of this condition can be directly verified by substituting the above definitions into Eq. (16).

The calculations carried out below assume the adiabatic approximation with respect to the weak z dependence of the background density and velocity. This means that their derivatives with respect to z are discarded, except for nonadiabatic corrections (21) and (22). We also take the curvature $1/r_h$ of the event horizon into account. The z nonstationarity and curved horizon are essential corrections and constitute important differences with respect to the analysis carried out in Refs. [52,58]. Another assumption is that the position of the black horizon does not vary with z. Varying Eq. (17) with respect to z and using Eq. (16) we can understand that this assumption works well if the black horizon lies in the vicinity of the optimal radius

$$r_{\rm opt} = \sqrt{\frac{|n|+1}{2}}\, w_0, \tag{25}$$

then $\alpha_s = 2/r_h$. For the parameters used above we can estimate the corresponding vorticity as $n_{\rm opt} \approx 22$.

The starting point of our analysis is then Eqs. (3), which we now expand with respect to the small parameters $\alpha_{s,r}x \ll 1$ and $x/r_h \ll 1$. Moreover, we take the Fourier transform of the field fluctuations $\chi(x,\phi,z)$ and $\xi(x,\phi,z)$; namely,

$$\chi(x,\phi,z) = \sum_m \int d\nu \int dk\, \chi_{k,m,\nu} e^{i(\nu z - m\phi - kz)}, \tag{26}$$

thus obtaining the following set of coupled equations for the Fourier components of the field fluctuations

$$\begin{pmatrix} \mathcal{A}_m(k) & \mathcal{B}_m(k) \\ \mathcal{C}_m(k) & \mathcal{A}_m(k) \end{pmatrix} \begin{pmatrix} \chi_{k,m,\nu} \\ \xi_{k,m,\nu} \end{pmatrix} = 0, \tag{27}$$

where

$$\tilde{\nu}_m = \frac{1}{s_h}\left(\nu - \frac{mn}{\beta_0 r_h^2}\right), \tag{28}$$

is the normalized vortex-corrected frequency and the matrix elements $\mathcal{A}_m(k)$, $\mathcal{B}_m(k)$, and $\mathcal{C}_m(k)$ are given by

$$\mathcal{A}_m(k) = i(\widetilde{\nu}_m - k) - i\alpha_r \partial_k k, \tag{29a}$$

$$\mathcal{B}_m(k) = \frac{1}{\beta_0 s_h}\left[(-\alpha_s + 1/r_h)ik + k^2 + \frac{m^2}{r_h^2}\right], \tag{29b}$$

$$\mathcal{C}_m(k) = -\frac{1}{4}\mathcal{B}_m(k) - s_h\beta_0(1 + i\alpha_s\partial_k). \tag{29c}$$

Following the procedure detailed in Appendix C, the solution of Eq. (27) can be written as

$$\chi(x,m,z) = e^{i(-m\phi+\nu z)} F(\tilde{\nu},x), \tag{30}$$

where

$$F(\tilde{\nu},x) = \int_C dk\, k^{\gamma_1}\left(k - \frac{2\widetilde{\nu}}{3}\right)^{\gamma_2} e^{\Lambda_0(k,\widetilde{\nu}) - ikx}, \tag{31}$$

with the definitions

$$\gamma_1 = \frac{i\widetilde{\nu}_m}{2\alpha_r} - \frac{im^2}{2r_h{}^2\widetilde{\nu}_m\alpha_r} + O\left(l_n^2/r_h^2\right), \tag{32a}$$

$$\gamma_2 = \left[\frac{\alpha_s - \alpha_r}{\varrho} - \frac{1}{r_h\varrho} - \frac{i\widetilde{\nu}_m}{2\alpha_r} + \frac{2\,i\widetilde{\nu}_m}{\varrho} + \frac{im^2}{2r_h^2\widetilde{\nu}_m\alpha_r}\right] + O\left(l_n^2/r_h^2\right), \tag{32b}$$

$$\Lambda_{m,\nu}(k) = \frac{k^3 l_n^2}{\varrho}\left[\frac{i}{6} + \frac{i}{2kr_h} + \frac{i\widetilde{\nu}\alpha_r}{2k\varrho} + \frac{\alpha_s}{2k} + O(1/(kr_h)^2)\right]. \tag{32c}$$

In the expressions above, $l_n^2 = 1/(\beta_0 g\rho)$ ($l_n \approx 10^{-5}$ m for the above parameters) is the so-called nonlinearity length, akin to the healing length in BEC [58], and $\varrho = 2\alpha_r + \alpha_s$. At $r_{\rm opt}$ we get $\varrho = 4/r_{h+}$. Only the leading terms are retained in Eqs. (32). The full expressions are given in Appendix C. The convergence of the above integral is controlled by the cubic term in the exponential. As a result, one can find four independent contours of integration, corresponding to four independent solutions of Eq. (27). The integral in Eq. (31) can be solved by using the steepest descent technique. The equation for the saddle points then reads

$$\left[(\widetilde{\nu}s_h - kv_r(x))^2 - ik(\alpha_r - \alpha_s + 1/r_h) - \frac{m^2}{r_h^2}\right] = \frac{l_n^2}{2}\left[(-\alpha_s + 1/r_h)ik + k^2 + \frac{m^2}{r_h^2}\right]^2 + k^2 s(x)^2. \tag{33}$$

The first two saddle points can be obtained in the limit of small k, when the terms $O(l_n^2)$ in Eq. (33) can be neglected. This results in one singular and one regular solution. The singular solution is

$$k_s = \frac{2\widetilde{\nu}_m s_h - i(\alpha_r - \alpha_s + 1/r_h)}{x\varrho} \propto \frac{1}{x}, \tag{34}$$

and corresponds to $\chi_s = x^{\gamma-1}$, where, to the leading order,

$$\gamma = -\gamma_1 - \gamma_2 = \gamma_a + \gamma_0 + O\left(l_n^2\right), \tag{35}$$

with

$$\gamma_a = \frac{\alpha_r - \alpha_s}{\varrho} + \frac{1}{r_h\varrho} = \frac{(|n|-1)w_0^2 - 2r_h^2}{-2r_h^2 + w^2(|n|+1)}, \tag{36a}$$

$$\gamma_0 = -\frac{2\,i\widetilde{\nu}_m}{\varrho}. \tag{36b}$$

The second saddle point is given by

$$k_r = \frac{\widetilde{\nu}_m^2 s_h^2 - m^2/r_h^2}{2\widetilde{\nu}_m s_h^2 + i(\alpha_r - \alpha_s + 1/r_h)}$$

and corresponds to the regular solution $\chi \propto e^{-ik_r x}$. Together with the regular and singular solutions displayed above, there are two more solutions, corresponding to evanescent states in the subsonic region II in Fig. 3. These solutions, however, become propagating in the supersonic regions I and III. To find them we have to consider the limit of large k, $kl_n \gg 1$, at $x > \alpha l_n^2$. Then, Eq. (33) becomes

$$\frac{l_n^2}{2}k^3 - k\varrho x = 0. \tag{37}$$

This equation admits two solutions; namely,

$$k_{e1,2} = \pm\sqrt{2\varrho x/l_n^2}, \tag{38}$$

which correspond to the functions

$$\chi_{e1,2} \propto \exp\left(\pm i\frac{\sqrt{2\varrho}}{3l_n}x^{3/2}\right). \tag{39}$$

Finally, we carry out the transformation given by Eq. (8) and use the relation between the functions χ and ξ to obtain the following triads of incoming waves:

$$\xi_{r1}(x) = |x|^{-\gamma_0/2}e^{i\nu z - im\phi}, \quad x<0, \tag{40a}$$

$$\xi_{r2}(x) = x^{-\gamma_0/2}e^{i\nu z - im\phi}, \quad x>0, \tag{40b}$$

$$\xi_{e1}(x) = \sqrt{\frac{4l_n\widetilde{\nu}_m}{(\varrho\bar{x})^{3/2}}}\tilde{x}^{\gamma_0/2}e^{i\nu z - im\phi + i\frac{\sqrt{2\varrho}}{3l_n}x^{3/2}}, \tag{40c}$$

and outgoing waves

$$\xi_{s1}(x) = |x|^{\gamma_a+\gamma_0/2}e^{i\nu z - im\phi}, \quad x<0, \tag{41a}$$

$$\xi_{s2}(x) = x^{\gamma_a+\gamma_0/2}e^{i\nu z - im\phi}, \quad x>0, \tag{41b}$$

$$\xi_{e1}(x) = \sqrt{\frac{4l_n\widetilde{\nu}_m}{(\varrho\bar{x})^{3/2}}}\tilde{x}^{\gamma_0/2}e^{i\nu z - im\phi - i\frac{\sqrt{2\varrho}}{3l_n}x^{3/2}}. \tag{41c}$$

Note that the eigenfunctions ξ_r and ξ_s are propagating in both the subsonic (II) and supersonic (I and III) regions, whereas the eigenfunctions ξ_{1e} and ξ_{2e} are propagating only in the supersonic regions. A detailed discussion of interrelation between these solutions is presented in Refs. [52,58] for the linear z-stationary flow background, and the analysis of the scattering problem outlined there can be fully applied to the present case. Although the eigenfunctions presented here are formally similar to those of Refs. [52,58] (see also Refs. [59–62] for an analysis related to the Schwarzschild black hole), there are two important differences. First, the singular eigenfunctions $\xi_{s1,s2}$ acquire now an extra factor $|x|^{\gamma_a}$, where

$$\gamma_a = \frac{2(r_m^2 - r_h^2) - w_0^2}{2(r_m^2 - r_h^2) + w_0^2}, \tag{42}$$

$r_m^2 = |n|w_0^2/2$ being the maximum of the Laguerre–Gaussian beam. The quantity γ_a may be either positive or negative, depending on the parameters, which leads either to an increasing density of fluctuations when approaching the horizon if $\gamma_a < 0$, or to a suppression of the fluctuation density near the horizon if $\gamma_a > 0$. One also must not forget that this description holds for $|x| > l_n$. Figure 4 shows γ_a for the outer black horizon $h+$ as a function of the focal length f of the diverging lens (i.e., as a function of the radial flow). For the outer horizon, $r_m < r_{h+}$ and therefore the numerator in Eq. (42) is always negative, whereas the denominator can be zero and change its sign at $r_{\rm opt}$, Eq. (25). As a result, there exists a critical value of the focal length f (corresponding to a critical value of the radial flow) where γ_a has a vertical asymptote (i.e., it diverges and also changes its sign). For negative γ_a in this region, the fluctuation density becomes strongly skewed towards the outer event horizon. For the inner event horizon, on the other hand, $r_m > r_{h-}$ and it is the numerator that goes to zero when γ_a changes its sign. Therefore, no divergence is observed in this case.

The second important distinction is connected with the fact that expression (28) for the frequency $\widetilde{\nu}$ contains the term

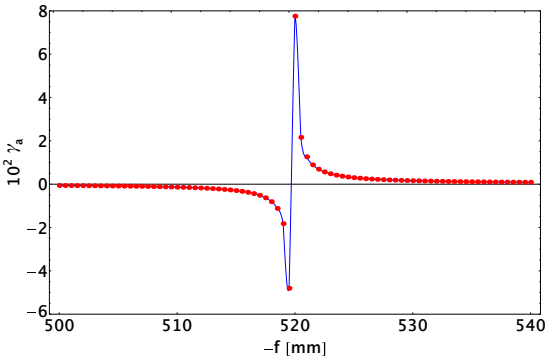

FIG. 4. γ_a as a function of the focal length f for the outer horizon. The red dots correspond to the actual numerical value of γ_a, while the blue solid line is a spline interpolation. As can be seen, in the vicinity of the critical focal length $f_c \simeq 520$ mm, γ_a shows a typical resonant behavior. Note that, while Eq. (42) contains an actual divergence for $f = f_c$, in the interpolation shown in this picture, this does not appear because it is instead replaced by a resonance. The divergence, in fact, is an artifact of the approximated analysis carried out to obtain Eq. (42) and it is not present if the full solution is taken into account. The radial intensity profile of the vortex, with vorticity $n = 6$, corresponds to $I = 2$W, $g = 5.5\times10^{-4}$ m/W, $w_0 = 1$ mm, and $\beta_0 = (2\pi/7.80)\times10^7$ m^{-1}.

reflecting the vorticity m of the mode as well as the vorticity n of the background. A similar problem in the GR context for the Kerr–Newman black hole is discussed in Refs. [3,63–66]. In particular, $\widetilde{\nu}$ can become negative, which implies SR. To get the spectrum of Hawking radiation we have to carry out the transformation given by Eq. (8) and solve the scattering problem, in a similar manner as explained in detail in Ref. [52]. Following the procedure highlighted in Appendix C, we finally get

$$N(\nu) = [e^{\pi\,\mathrm{Im}\{\gamma\}} - 1]^{-1}, \tag{43}$$

where

$$\mathrm{Im}\{\gamma\} = \frac{2\tilde{\nu}}{s_h\varrho} = \frac{2}{s_h\varrho}\left(\nu - \frac{nm}{\beta_0 r_h^2}\right). \tag{44}$$

The corresponding Hawking temperature is then given by

$$T_H(\nu) = \frac{\hbar s_h\varrho}{2\pi k_B}, \tag{45}$$

where k_B is the Boltzmann constant.

As outlined in Ref. [3] (see also Ref. [67]) the spectral density of the Hawking radiation has to overcome a barrier before being registered by distant observer. In our analog case, in principle, we can observe the radiation before it penetrates the barrier. Moreover, the barrier does not necessarily exist (see Appendix B).

Resonant enhancement of Hawking radiation

The situation when $\widetilde{\nu}$ is close to zero, i.e., when $\nu \sim nm/(\beta_0 r_{h+}^2)$, is of a special interest, since we expect the radiation to be strongly enhanced in this spectral region. When $\widetilde{\nu}$ changes its sign the outgoing wave becomes incoming [see Eq. (B5)] and vice versa. Therefore we have to change the

sign in Eq. (36b). Then, by keeping the leading-order term in Eq. (43), we have

$$N(\nu) = \frac{s_{h_+}\varrho}{2\pi|\nu - \nu_+|}. \tag{46}$$

The condition $\widetilde{\nu} = 0$ can be rewritten in the form

$$m\lambda_\nu = \tau_\phi, \tag{47}$$

where $\lambda_\nu = 2\pi/\nu$ and $\tau_\phi = 2\pi r_h/v_\phi$, and v_ϕ is the azimuthal component of the velocity flow. The above expression can be interpreted as a typical resonance condition, which happens when an integer number m of wavelengths λ_ν coincides with the propagation distance τ_ϕ necessary for one full rotation of the vortex. This condition is also related to the SR, since it corresponds to the total reflection [see Eq. (B9)]. This resonance condition can strongly enhance the otherwise exponentially weak Hawking radiation at certain frequencies, and makes its experimental observation feasible. It should be noted here that the exact resonance is not reachable due to the condition (B6).

To understand why this is true, one should realize that, in order to establish quasistationary conditions and avoid a strong z dependence of the position of the horizon and the physical parameters there, the cell containing the nonlinear medium should be significantly shorter than the local length f. This sets a lower limit on the frequency of Hawking radiation that such a cell can emit; namely, $\lambda_c = 2\pi/\nu_c < f$. In the absence of vorticity, $n = 0$ when $\varrho \approx 4/r_h$, the spectral weight of the emitted frequency components is exponentially small:

$$N(\nu_c) \propto e^{-\frac{\nu_c}{\nu_H}} = e^{-\frac{\pi^2 f}{\lambda_c}}, \tag{48}$$

where

$$\nu_H = \frac{2\pi}{\lambda_H} = \frac{s_h\varrho}{2\pi} \approx \frac{2}{\pi f}. \tag{49}$$

This situation may drastically change in the case of a vortex with a sufficiently high vorticity n, since near the critical frequency,

$$\left|\nu - \frac{nm}{\beta_0 r_h^2}\right| \sim \frac{1}{\lambda_H}, \tag{50}$$

the radiation intensity would not contain the exponentially small factor anymore. One can readily estimate that, in order to obtain a resonance at $\lambda_r = 2\pi/\nu_r \approx 10$ cm (which is a typical propagation length for realistic experimental parameters), the condition

$$\lambda_\nu \approx \frac{2\pi\beta_0 r_h^2}{nm} \approx \frac{\pi\beta_0 w_0^2(n+1)}{nm} \tag{51}$$

must be satisfied. Using Eq. (25) the vorticity n drops out at large n and Eq. (51) becomes a condition on m. If we substitute the parameters used in Fig. 1 we get that m should be larger than a couple of hundred, which does not seem to be experimentally realistic. However, by choosing smaller values of β_0 and w_0, say, by a factor of two or so, we can readily gain an order of magnitude or more. This means that we can arrive at the condition $m < 10$ which is challenging but should be feasible considering the state of the art of vortex beam generation techniques. Then, instead of the exponentially small signal (48), we may expect a much stronger signal.

VI. SUMMARY AND CONCLUSIONS

In this work, we have used a coherent Laguerre–Gaussian beam propagating in a defocusing Kerr nonlinear medium as a model system for observation of the analog Hawking radiation. Our approach is based on the hydrodynamic formulation of the propagation of light in a nonlinear medium [see Eqs. (2)] and is therefore formally analogous to the dynamics of a compressible inviscid liquid. Compared to other models dealing with vortices, our model has the advantage of admitting nonzero radial flow by simply placing a diverging lens in font of the nonlinear medium itself. The diverging lens, in fact, induces a nonzero phase front curvature proportional to r/f [see Eq. (14b)], which allows for a control of the radial flow and allows the formation of an event horizon in our model. The geometry induced by this vortex background gives rise to the situation depicted in Fig. 3, where a white (h_-) and black (h_+) event horizon appear, together with two corresponding ergoregions (e_- and e_+, respectively).

Considering the Hawking radiation from the (black) event horizon, we have shown that the vorticity of the background and of the field fluctuations compete to create a resonant amplification of the emitted Hawking radiation [see Eq. (46)]. Accounting for the leading nonadiabatic (i.e., slowly z dependent) corrections result in important features of the fluctuations, such as their enhancement or suppression in the vicinity of the horizon, whose magnitude can be controlled experimentally by varying the focal length of the diverging lens in the proposed experimental setup.

The most interesting feature is the prediction of a resonance condition which may significantly amplify the otherwise extremely weak Hawking radiation in the relevant spectral interval. The same resonance condition controls the onset of SR, with total reflection taking place exactly at the resonance. Our estimates show that satisfying the conditions for experimental observation of the resonance, while challenging, is nevertheless a feasible task. We should also indicate that our estimates favor higher vorticities when some of the approximations used in the paper become less reliable. A different approach will then be necessary.

ACKNOWLEDGMENTS

The authors are indebted to the German–Israeli Foundation. M.O. is thankful to the Raymond and Beverly Sackler Faculty of Exact Sciences at Tel Aviv University for kindly hosting him while working on this project. V.F. acknowledge the hospitality of the Center for Theoretical Physics of Complex Systems, Daejeon, South Korea, where part of this project was performed. The authors thank the Deutsche Forschungsgemeinschaft (Grant BL 574/13-1) for financial support. Discussions with N. Pavloff and B. Reznik are highly appreciated.

APPENDIX A: INTRODUCTION OF RADIAL FLOW IN LAGUERRE–GAUSSIAN BEAM

In this Appendix we explicitly derive Eqs. (14) by using standard Gaussian optics. Let us consider the ABCD matrix describing the propagation of a Laguerre–Gaussian beam whose waist ($z = 0$) coincides with the position of a defocusing lens of focal length $-f$. The input plane of the nonlinear

medium is a short distance z behind the lens. Thus

$$\begin{pmatrix} A & B \\ C & D \end{pmatrix} = \begin{pmatrix} 1 & z \\ 0 & 1 \end{pmatrix}\begin{pmatrix} 1 & 0 \\ 1/f & 1 \end{pmatrix}. \tag{A1}$$

We then use the self-similarity of the Gaussian q parameter, i.e.,

$$q'(z) = \frac{Aq(0)+B}{Cq(0)+D}, \tag{A2}$$

to calculate the beam parameters. Recalling that

$$\frac{1}{q(z)} = \frac{1}{R(z)} - i\frac{2}{\beta w^2(z)}, \tag{A3}$$

we can calculate the beam waist and the beam curvature at a distance z from the lens, assuming that this distance is small compared with the Rayleigh range z_R of the beam itself. Note that, in the paraxial approximation, this condition is easily satisfied, because the typical value of z_R for a collimated beam of a few mm diameter is on the order of several meters. We therefore have, in the limit of small z,

$$w^2(z) \simeq \frac{f w_0^2}{f-2z}, \tag{A4}$$

$$\frac{1}{R(z)} \simeq \frac{1}{f}. \tag{A5}$$

If we now substitute these equations in the expressions for ρ and $\mathbf{v}$ given by Eqs. (10), and expand those in the limit of small z, we obtain the expressions used in Sec. III.

APPENDIX B: SUPERRADIANCE

In this Appendix, we investigate the occurrence of SR in the scattering of electromagnetic fluctuations from the ergoregion. This effect has been discussed in GR [68–70] and in several analog systems [55,56,71], including optical ones [13,14]. The situation in our case is somewhat different since we deal now with the subsonic region sandwiched between two supersonic regions. Here, we will discuss propagation of the fluctuation in our system, leaving the detailed analysis for the future. The metric defined in Eq. (9) allows us to write the differential equation in tortoise coordinates for the field fluctuation $\xi = \bar{\xi}\, e^{i\nu z - im\phi}$ as follows:

$$\frac{D}{r}\partial_r r D \partial_r \bar{\xi} + \widetilde{\nu}_m(r)^2\bar{\xi} - \frac{m^2 D}{r^2}\bar{\xi} - \frac{i\widetilde{\nu}_m(r)}{s}[\partial_z \ln(s^2 D)]\bar{\xi} = 0, \tag{B1}$$

where $D = (s^2 - v_r^2)/s^2$. The last term in Eq. (B1) accounts for the nonadiabatic evolution due to the z dependence of the vortex profile. It also causes a weak dependence of $\bar{\xi}$ on z. However, this nonadiabatic correction can be shown to be of order $1/(\nu z_R) \ll 1$ and can therefore be neglected in our analysis. Moreover, the divergence at $r \to r_h$ and $D \to 0$ occurs in a narrow region where a regularization procedure (such as the one outlined in Sec. V) should be applied. Introducing the new coordinate $dr_* = D^{-1}dr$ and the new function $\psi = r^{1/2}\bar{\xi}$, Eq. (B1) becomes

$$-\partial_{r_*}^2\psi + V(r(r_*))\psi = 0, \tag{B2}$$

where $V(r(r_*))$ is the effective potential, whose explicit expression reads

$$V(r(r_*)) = -\widetilde{\nu}_m(r)^2 + \frac{m^2 D}{r^2(r_*)} - \frac{1}{4}\frac{d}{dr}\left[\frac{D^2}{r(r_*)}\right]. \tag{B3}$$

A closer inspection of the above equation reveals that the effective potential has two r_*-independent asymptotes; namely,

$$V(r) \to -\frac{1}{s^2}(\nu - \nu_\pm)^2 \quad \text{at } r \to r_{h_\pm}, \tag{B4}$$

where

$$\nu_\pm = \frac{mn}{\beta_0 r_{h_\pm}^2}.$$

We are interested in studying the processes related to the black horizon ($r \to r_{h_+}$) and how they are influenced by the boundary conditions at the white horizon ($r \to r_{h_-}$). This issue is discussed below. We first calculate the wave function in the eikonal approximation. For this we look for a solution in the form $\psi = ue^{iS}$. Then in the leading order in $S \gg 1$ we get

$$\overline{\psi} = \frac{Ce^{i(\nu z - m\phi)}}{\sqrt[4]{-V(r_*)}} \exp\left[\pm i\int_r^{r_{h_+}-l_r}\sqrt{-V(r_*)}dr_*\right], \tag{B5}$$

where C is the normalization constant, and l_r is the regularization length, defined in Eq. (C6). In the limit $r \to r_{h_+}$ we may write $D = \varrho(r - r_{h_+})$ and, from the equation above, we may straightforwardly get that

$$\xi \sim e^{\pm i\frac{(\nu-\nu_+)}{\varrho s}\ln\frac{|r-r_{h+}|}{l_r}},$$

which corresponds to the functions in Eqs. (40a) and (41a). This conclusion assumes that there is an area $r_{h_+} > r > l_r$ near the black horizon where $V(r) < 0$. If we use Eq. (25), the condition $V(r) < 0$ corresponds to the following condition on the frequency ν:

$$(\nu - \nu_+)^2 > s_{h_+}^2\frac{\varrho^2 l_r^2}{w^2}\frac{2(m^2+n+1)}{2n+1}. \tag{B6}$$

The coordinate-dependent wave vector of the wave (B5) is

$$k^2(r) = -\frac{V(r)}{D^2(r)}. \tag{B7}$$

Depending on the sign of the potential $V(r)$ it may be real, corresponding to the propagating waves, or imaginary, corresponding to the evanescent states. The actual situation is very sensitive to the parameters of the system. Figure 5 shows $k(r)^2$ in region II in three possible regimes: for $m = 2$ (dashed, black line) $k(r)^2 > 0$ in the whole region II, and that the wave can freely propagate in the subsonic region II. If the vorticity of the fluctuation is increased slightly to $m = 3$, corresponding to the solid, blue line in Fig. 5, a region where $k(r)^2 < 0$ appears, i.e., there is a barrier which can either reflect or transfer the wave. This region corresponds to the values of the radial coordinate in the interval $2.73 < r < 3.35$ mm (shaded blue region). Finally, if the vorticity of the fluctuation is increased further to $m = 6$, the barrier is so high and broad that it covers nearly the whole region II; however, there remains a small area ($r > 3.78$ mm) near the black horizon where $k(r)^2 > 0$.

The case with a barrier inside the region II presents a special interest. Consider a wave propagating from the black

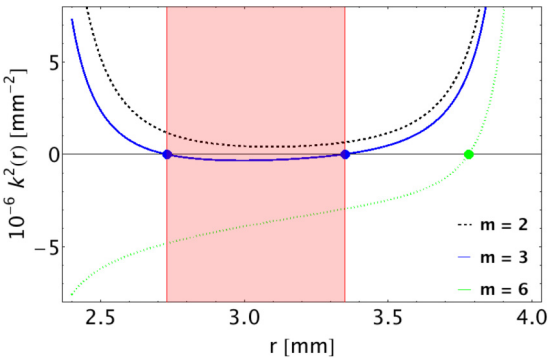

FIG. 5. The squared wave vector $k^2(r)$ in the subsonic region II for the parameters $I = 2$ W, $g = 5.5\times10^{-4}$ m/W, $w_0 = 1$ mm, $\beta_0 = (2\pi/7.80)\times10^7$ m^{-1}, and $f = 6$ m. The vorticity of the beam is chosen $n = 20$ then $r_{h_-} = 0.925$ mm and $r_{h_+} = 3.03$ mm. We assume that the registered frequency of the fluctuation is $\nu = 3$ m^{-1} and we consider also three possible vorticities of the emitted radiation: for $m = 2$ (black, dashed line) the graph is everywhere positive, corresponding to propagating wave with $k(r) > 600$ m^{-1}. For $m = 3$ (solid, blue line) there is a barrier in the middle of the region II where the wave becomes evanescent. For $m = 6$ (dotted, green line) the barrier becomes high and broad and covers the most part of the region II, thus leaving a narrow area near the black horizon free. The shaded red region, encapsulated by the two red dots corresponding to $r = 2.73$ mm and $r = 3.35$ mm, corresponds to the region (for the case $m = 3$), where the wave vector is evanescent, i.e., $k^2(r) < 0$. The green dot at $r = 3.78$ mm corresponds to the starting point of the region in which the wave vector for $m = 6$ corresponds to a propagating wave, i.e., $k^2(r) > 0$.

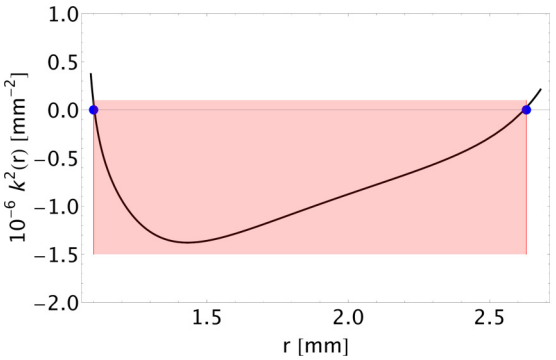

FIG. 6. The squared wave vector $k^2(r)$ in the subsonic region II for the parameters: $I = 2$ W, $g = 5.5\times10^{-4}$ m/W, $w_0 = 1$ mm, $\beta_0 = (2\pi/7.80)\times10^7$ m^{-1}, and $f = 6$ m. The vorticity of the beam is chosen $n = 9$, so that $r_{h_-} = 0.925$ mm and $r_{h_+} = 3.03$ mm. Under these conditions, the resonance frequencies are $\nu_- = 5.803\,516\,989$ m^{-1} and $\nu_+ = 0.540\,865\,734\,7$ m^{-1}, respectively. We assume that the registered value of the fluctuation is $\nu = 2$ m^{-1}. Here, $m = 2$ and the potential forms a barrier, reaching the value $V(r_m) = 8\times10^5$ m^{-2} in its maximum not far from the midpoint $r_m = (r_{h_+} - r_{h_-})/2$ of region II. The light red box in the figure shows the region where the wave vector is evanescent; namely, $k^2(r) < 0$.

horizon towards the barrier. The effective potential has two r_*-independent asymptotes (B4). Corresponding to the asymptotic limits for the potential $V(r(r_*))$, the wave function $\psi(r_*)$ can be written as follows:

$$\psi(r_{*+}) = e^{i(\nu-\nu_+)r_{*+}} + \mathrm{Re}^{-i(\nu-\nu_+)r_{*+}} \quad \text{at } r \to r_{h_+}, \tag{B8a}$$

$$\psi(r_{*-}) = Te^{i(\nu-\nu_-)r_{*-}} \text{ at } r \to r_{h_-}, \tag{B8b}$$

where R and T are reflection and transmission amplitudes, respectively. To calculate the relation existing between R and T, we observe that, since Eq. (B2) does not contain first derivatives, then, according to Abel's theorem, its Wronskian is constant [72]. Therefore, by equating the Wronskians calculated for the two above limits by means of the functions (B8a) and (B8b) and their complex conjugate, we get the following relation:

$$1 - |R|^2 = |T|^2 \frac{\nu - \nu_-}{\nu - \nu_+}. \tag{B9}$$

Note that the same condition can also be obtained by balancing the ingoing and outgoing currents on both sides of the barrier using Eq. (C9b) and the function (B5). If we consider the case $\nu_- < \nu < \nu_+$ as in Fig. 6, the right-hand side of Eq. (B9) is negative, i.e., the transmission coefficient

$$\mathcal{T}_+ = |T|^2 \frac{\nu - \nu_-}{\nu - \nu_+} \tag{B10}$$

is negative. In this case, the reflection coefficient $\mathcal{R} = |R|^2$ becomes larger than one, meaning that the reflected wave is stronger than the incident wave, i.e., that the former is amplified. At $\nu \to \nu_+$ we can readily get that $|T|^2 \to 0$. Considering a fluctuation prorogating from the white horizon towards the barrier we get the transmission coefficient in the form

$$\mathcal{T}_- = |T|^2 \frac{\nu - \nu_+}{\nu - \nu_-}. \tag{B11}$$

Although this is similar to the superradiance of a Kerr black hole, there are important dissimilarities. The central point is that the distant observer of the astronomical black hole should be now placed near the sphere of the white horizon. We may also consider the radiation in the area between the black horizon and the barrier, which is not observable otherwise. An interesting possibility of creating a regime similar to the "black-hole bomb" [73] deserves a special consideration.

APPENDIX C: NONADIABATIC CORRECTIONS

The coefficients in Eqs. (3) and (4) derived in the main text depend on z. However, their derivation did not require any sort of adiabatic approximation. The necessity of applying an adiabatic approximation and investigating nonadiabatic corrections arises only when looking for solutions of these equations. It is the aim of this Appendix to present this analysis taking into account the quantum potential. We give here the full expressions for the quantities appearing in Eqs. (32), rather than only their leading order in l_n^2. We apply the expansion outlined in Sec. V and then carry out the Fourier transform of $\chi(x,\phi,z)$; namely,

$$\chi(x,\phi,z) = \sum_m \int d\nu \int dk\, \chi_{k,m,\nu}\, e^{i(\nu z - m\phi - kz)}. \tag{C1}$$

Substituting this into Eqs. (3), we obtain Eqs. (27). We can now solve the first of Eqs. (27) with respect to $\xi_{k,m,\nu}$ and substitute

the result into the second of Eqs. (27), thus obtaining

$$\partial_k \ln \chi_{k,m,\nu} = \frac{i\left[\widetilde{\nu}_m^2 - 2\widetilde{\nu}_m k - ik(\alpha_r - \alpha_s + 1/r_h) - \frac{m^2}{r_h^2}\right]}{k[2\widetilde{\nu}_m\alpha_r - k(\alpha_s + 2\alpha_r)]} - \frac{il_n^2}{2}\frac{\left[(-\alpha_s + 1/r_h)ik + k^2 + \frac{m^2}{r_h^2}\right]^2}{k[2\widetilde{\nu}_m\alpha_r - k(\alpha_s + 2\alpha_r)]}, \tag{C2}$$

where $l_n^{-2} = 2\beta_0^2 s_h^2$ is the nonlinearity length. If we now integrate the above equation, we can write the solution in the following form:

$$\chi_{m,\nu} = e^{i(-m\phi+\nu z)}F(\tilde{\nu},x), \tag{C3}$$

where $F(\tilde{\nu},x)$ is given by Eq. (31) and reads

$$F(\tilde{\nu},x) = \int_C dk\, k^{\gamma_1}\left(k - \frac{2\widetilde{\nu}}{3}\right)^{\gamma_2} e^{\Lambda_{m,\nu}(k) - ikx}. \tag{C4}$$

The exact expressions for γ_1, γ_2, and $\Lambda_{m,\nu}(k)$ are reported below for the sake of completeness:

$$\gamma_1 = \frac{i\widetilde{\nu}_m}{2\alpha_r} - \frac{im^2}{2{r_h}^2\widetilde{\nu}_m\alpha_r} - \frac{i{l_n}^2m^4}{4{r_h}^4\widetilde{\nu}_m\alpha_r}, \tag{C5a}$$

$$\gamma_2 = \left[\frac{\alpha_s - \alpha_r}{\varrho} - \frac{1}{r_h\varrho} - \frac{i\tilde{\nu}_m}{\varrho} + \frac{2i\tilde{\nu}_m}{\varrho} + \frac{im^2}{2r_h^2\tilde{\nu}_m\alpha_r}\right] + l_n^2\left[\frac{i\tilde{\nu}_m\alpha_r}{r_h^2\varrho^2} + \frac{im^4}{4r_h^4\tilde{\nu}_m\alpha_r} + \frac{4i\tilde{\nu}_m^2\alpha_r^2}{r_h\varrho^3} + \frac{4\alpha_r^2\tilde{\nu}_m^2}{\varrho^2} - i\tilde{\nu}_m\alpha_r - \frac{2\alpha_r m^2}{r_h^2\varrho} - \frac{4\tilde{\nu}_m\alpha_r^2}{r_h\varrho^2} + \frac{2\tilde{\nu}_m\alpha_r}{r_h\varrho} + \frac{im^2}{r_h^3\varrho} + \frac{4i\tilde{\nu}_m^3\alpha_r^3}{\varrho^4} - \frac{4i\tilde{\nu}_m\alpha_r^3}{\varrho^2} + \frac{4i\tilde{\nu}_m\alpha_r^2}{\varrho} + \frac{m^2}{r_h^2} - \frac{8\tilde{\nu}_m^2\alpha_r^3}{\varrho^3} + \frac{2i\tilde{\nu}_m\alpha_r l^2m^2}{r_h^2\varrho^2}\right], \tag{C5b}$$

$$\Lambda_{m,\nu}(k) = \frac{k^3l_r^3}{3}\left[\frac{i}{6} + \frac{i}{2kr_h} + \frac{i\widetilde{\nu}\alpha_r}{2k\varrho} + \frac{\alpha_s}{2k} + \frac{2i\alpha_r\nu}{k^2r_h\varrho} + \frac{2\alpha_r\alpha_s\widetilde{\nu}}{k^2\varrho} + \frac{i}{2k^2r_h^2} + \frac{im^2}{k^2r_h^2} + \frac{2i{\alpha_r}^2\widetilde{\nu}^2}{k^2\varrho^2} + \frac{\alpha_s}{k^2r_h} - \frac{i\alpha_s^2}{2k^2}\right], \tag{C5c}$$

with

$$l_r = l_n(\varrho l_n/3)^{-1/3} \tag{C6}$$

being the regularization length [58] for the z-nonstationary flow. The quantum potential corrections are important at $|x| < l_r$ and negligible otherwise.

Normalization of Eigenfunctions

The goal of this Appendix is to derive the normalization constant of the eigenfunctions ξ and χ and show that it depends, in the case of a vortex background, on the sign of $\tilde{\nu}$. To do this we rely on the approach described in Ref. [58] and define the two-component field

$$\psi = \begin{pmatrix} \frac{\chi}{\sqrt{2}} \\ \sqrt{2}\xi \end{pmatrix}. \tag{C7}$$

Using standard field theory, we express the density and current associated with the field ψ as follows:

$$\rho^c = if_0^2(\xi^*\chi - \chi^*\xi), \tag{C8a}$$

$$\mathbf{j}^c = \rho^c\mathbf{v} - i\frac{f_0^2}{\beta_0}\left(\frac{1}{4}\chi^*\boldsymbol{\nabla}_\perp\chi + \xi^*\boldsymbol{\nabla}_\perp\xi - \text{c.c.}\right). \tag{C8b}$$

We then use the relation $\chi = (1/gf_9^2)\widehat{\mathcal{D}}\xi$, which holds at $|x| > l_n$, write Eqs. (C8) in polar coordinates, and make the transformation (8), obtaining

$$\tilde{\rho}^c = i\frac{s^2}{s^2 - v_r^2}\left[\xi^*\left(\overleftrightarrow{\partial}_z + \frac{v_\phi}{r}\overleftrightarrow{\partial}_\phi\right)\xi\right], \tag{C9a}$$

$$\tilde{j}_r^c = i\left(v_r^2 - s^2\right)\xi^*\overleftrightarrow{\partial}_r\xi, \tag{C9b}$$

$$\tilde{j}_\phi^c = \xi^*\left[\frac{iv_\phi s^2}{s^2 - v_r^2}\overleftrightarrow{\partial}_z + \frac{s^2\left(v_0^2 - s^2\right)}{r\left(s^2 - v_r^2\right)}\overleftrightarrow{\partial}_\phi\right]\xi, \tag{C9c}$$

where the derivative operator $\overleftrightarrow{\partial}_x$ is defined as follows:

$$\psi^*\overleftrightarrow{\partial}_x\psi = \psi^*\partial_x\psi - \psi\partial_x\psi^*. \tag{C10}$$

We now use Eq. (C9a) to define the scalar product, and consequently the norm of the eigenfunctions:

$$\{\psi_k,\psi_k\} = \int d\tilde{r}\,\tilde{\rho}_k^c, \tag{C11}$$

where the subscript k indicates the type of solution we are considering; namely, regular (r), evanescent (e), or singular (s). We are particularly interested in the behavior of the singular solution close to the event horizon. Following the procedure described in Refs. [74,75], we write

$$N\left(\{\xi_{m,1s},\xi_{m,1s}\} + \{\xi_{m,2s},\xi_{m,2s}\}e_m^{\frac{2\pi}{s_h\varrho}\widetilde{\nu}}\right) = -\text{sign}(\widetilde{\nu}_m). \tag{C12}$$

Using the scalar product defined above, one can readily verify that

$$\{\xi_{m,1s},\xi_{m,1s}\} = \text{sign}(\widetilde{\nu}_m), \tag{C13}$$

and

$$\{\xi_{m,2s},\xi_{m,2s}\} = -\text{sign}(\widetilde{\nu}_m). \tag{C14}$$

Hence, the normalization constant N, which serves as a spectral density of the Hawking radiation, is

$$N = \left(e^{\frac{2\pi\widetilde{\nu}_m}{s_h\varrho}} - 1\right)^{-1}. \tag{C15}$$

It is worth mentioning that a similar result has been obtained in the context of GR as well; see Refs. [3,59,64–66].

[1] R. Howl, L. Hackermüller, D. E. Bruschix, and I. Fuentes, arXiv:1607.06666v2.
[2] W. G. Unruh, Phys. Rev. Lett. **46**, 1351 (1981).
[3] S. W. Hawking, Commun. Math. Phys. **43**, 199 (1975).
[4] S. W. Hawking, Phys. Rev. D **13**, 191 (1976).
[5] M. Visser, Class. Quantum Grav. **15**, 1767 (1998).
[6] T. A. Jacobson and G. E. Volovik, Phys. Rev. D **58**, 064021 (1998).
[7] B. Reznik, Phys. Rev. D **62**, 044044 (2000).
[8] S. Giovanazzi, Phys. Rev. Lett. **94**, 061302 (2005).
[9] C. Barcelo, S. Liberati, and M. Visser, Phys. Rev. A **68**, 053613 (2003).
[10] I. Carusotto, S. Fagnocchi, A. Recati, R. Balbinot, and A. Fabbri, New J. Phys. **10**, 103001 (2008).
[11] A. Recati, N. Pavloff, and I. Carusotto, Phys. Rev. A **80**, 043603 (2009).
[12] P. D. Nation, M. P. Blencowe, A. J. Rimberg, and E. Buks, Phys. Rev. Lett. **103**, 087004 (2009).
[13] F. Marino, Phys. Rev. A **78**, 063804 (2008).
[14] F. Marino, M. Ciszak, and A. Ortolan, Phys. Rev. A **80**, 065802 (2009).
[15] I. Fouxon, O. V. Farberovich, S. Bar-Ad, and V. Fleurov, Europhys. Lett. **92**, 14002 (2010).
[16] X. Busch, I. Carusotto, and R. Parentani, Phys. Rev. A **89**, 043819 (2014).
[17] P. Grišins, H. S. Nguyen, J. Bloch, A. Amo, and I. Carusotto, Phys. Rev. B **94**, 144518 (2016).
[18] G. Rousseaux, C. Mathis, P. Maissa, T. G. Philbin, and U. Leonhardt, New J. Phys. **10**, 053015 (2008).
[19] G. Rousseaux, P. Maissa, C. Mathis, P. Coulet, T. G. Philbin, and U. Leonhardt, New J. Phys. **12**, 095018 (2010).
[20] S. Weinfurtner, E. W. Tedford, M. C. J. Penrice, W. G. Unruh, and G. A. Lawrence, Phys. Rev. Lett. **106**, 021302 (2011).
[21] C. Peloquin, L.-P. Euve, T. Philbin, and G. Rousseaux, Phys. Rev. D **93**, 084032 (2016).
[22] L.-P. Euvé, F. Michel, R. Parentani, T. G. Philbin, and G. Rousseaux, Phys. Rev. Lett. **117**, 121301 (2016).
[23] G. Jannes, P. Maïssa, T. G. Philbin, and G. Rousseaux, Phys. Rev. D **83**, 104028 (2011).
[24] A. Roldán-Molina, A. S. Nunez, and R. A. Duine, Phys. Rev. Lett. **118**, 061301 (2017).
[25] T. G. Philbin, C. Kuklewicz, S. Robertson, S. Hill, F. König, and U. Leonhardt, Science **319**, 1367 (2008).
[26] F. Belgiorno, S. L. Cacciatori, M. Clerici, V. Gorini, G. Ortenzi, L. Rizzi, E. Rubino, V. G. Sala, and D. Faccio, Phys. Rev. Lett. **105**, 203901 (2010).
[27] O. Lahav, A. Itah, A. Blumkin, C. Gordon, S. Rinott, A. Zayats, and J. Steinhauer, Phys. Rev. Lett. **105**, 240401 (2010).
[28] J. Steinhauer, Nat. Phys. **12**, 959 (2016).
[29] J. Steinhauer, Nat. Phys. **10**, 864 (2014).
[30] S. Corley and T. Jacobson, Phys. Rev. D **59**, 124011 (1999).
[31] T. R. Slayter and C. M. Savage, Class. Quantum Grav. **22**, 3833 (2005).
[32] T. Torres, S. Patrick, A. Coutant, M. Richartz, E. W. Tedford, and S. Weinfurtner, Nat. Phys. **13**, 833 (2017).
[33] J. F. Nye and M. V. Berry, Proc. R. Soc. London, Ser. A **336**, 1605 (1974).
[34] L. Allen, M. W. Beijersbergen, R. J. C. Spreeuw, and J. P. Woerdman, Phys. Rev. A **45**, 8185 (1992).
[35] *The Angular Momentum of Light*, edited by D. L. Andrews and M. Babiker (Cambridge University Press, Cambridge, 2012).
[36] John Kerr discovered the nonlinear optical effect in 1875. Roy Kerr calculated the metric of a rotating black hole in 1963.
[37] W. Wan, S. Jia, and J. Fleischer, Nat. Phys. **3**, 46 (2007).
[38] G. A. El, A. Gammal, E. G. Khamis, R. A. Kraenkel, and A. M. Kamchatnov, Phys. Rev. A **76**, 053813 (2007).
[39] E. G. Khamis, A. Gammal, G. A. El, Yu. G. Gladush, and A. M. Kamchatnov, Phys. Rev. A **78**, 013829 (2008).
[40] G. Dekel, V. Fleurov, A. Soffer, and C. Stucchio, Phys. Rev. A **75**, 043617 (2007).
[41] M. Elazar, V. Fleurov, and S. Bar-Ad, Phys. Rev. A **86**, 063821 (2012).
[42] M. Elazar, S. Bar-Ad, V. Fleurov, and R. Schilling, in *An All-Optical Event Horizon in an Optical Analogue of a Laval Nozzle*, Analogue Gravity Phenomenology Lecture Notes in Physics (Springer, Berlin, 2013), Vol. 870, pp. 275–296.
[43] S. J. Robertson, J. Phys. B: At. Mol. Opt. Phys. **45**, 163001 (2012).
[44] I. Carusotto, Proc. R. Soc. London, Ser. A **470**, 20140320 (2014).
[45] R. Balbinot and A. Fabbri, Adv. High Energy Phys. **2014**, 713574 (2014).
[46] P.-E. Larré and I. Carusotto, Phys. Rev. A **92**, 043802 (2015).
[47] D. Vocke, T. Roger, F. Marino, E. M. Wright, I. Carusotto, M. Clerici, and D. Faccio, Optica **2**, 484 (2015).
[48] D. E. Bruschi, N. Friis, I. Fuentes, and S. Weinfurtner, New J. Phys. **15**, 13016 (2013).
[49] R. Boyd, *Nonlinear Optics*, 3rd ed. (Academic Press, Cambridge, 2008).
[50] E. Madelung, Eur. Phys. J. A **40**, 322 (1927).
[51] C. J. Pethick and H. Smith, *Bose–Einstein Condensates in Dilute Gases*, 2nd ed. (Cambridge University Press, Cambridge, 2008).
[52] Y. Vinish and V. Fleurov, Int. J. Mod. Phys. B **30**, 1650197 (2016).
[53] M. P. Hobson, G. P. Efstathiou, and A. N. Lazenby, *General Relativity: An Introduction for Physicists* (Cambridge University Press, Cambridge, 2006).
[54] L. D. Landau and E. M. Lifshitz, *Fluid Mechanics—Course on Theoretical Physics*, 2nd ed. (Butterworth-Heinemann Ltd., Oxford, 1987), Vol. 6.
[55] S. Basak and P. Majumdar, Class. Quantum Grav. **20**, 3907 (2003).
[56] M. Richartz, A. Prain, S. Liberati, and S. Weinfurtner, Phys. Rev. D **91**, 124018 (2015).
[57] F. L. Pedrotti and L. S. Pedrotti, *Introduction to Optics* (Pearson Education Limited, New York, 2013).
[58] V. Fleurov and R. Schilling, Phys. Rev. A **85**, 045602 (2012).
[59] S. Corley, Phys. Rev. D **57**, 6280 (1998).
[60] S. Corley and T. Jacobson, Phys. Rev. D **54**, 1568 (1996).
[61] A. Coutant, R. Parentani, and S. Finazzi, Phys. Rev. D **85**, 024021 (2012).
[62] X. Busch and R. Parentani, Phys. Rev. D **86**, 104033 (2017).
[63] S. Carlip, Class. Quantum Grav. **12**, 2853 (1995).
[64] K. Umetsu, Int. J. Mod. Phys. A **25**, 4123 (2010).
[65] I. Agullo, J. Navarro-Salas, G. J. Olmo, and L. Parker, Phys. Rev. Lett. **105**, 211305 (2010).
[66] K. Murata and J. Soda, Phys. Rev. D **74**, 044018 (2006).
[67] L. E. Parker and D. J. Toms, *Quantum Field Theory in Curved Spacetime* (Cambridge University Press, Cambridge, 2000).

[68] Ya. B. Zel'dovich, JETP **14**, 180 (1971).
[69] A. A. Starobinsky, Zh. Eksp. Teor. Fiz. **64**, 48 (1973) [english version: JETP **37**, 28 (1973)].
[70] W. G. Unruh, Phys. Rev. D **10**, 3194 (1974).
[71] R. Brito, V. Cardoso, and P. Pani, *Superradiance, Lecture Notes in Physics* (Springer-Verlag, Berlin, 2015), Vol. 906.
[72] F. W. Byron and R. W. Fuller, *Mathematics of Classical and Quantum Physics* (Dover, Mineola, NY, 2012).
[73] W. H. Press and S. A. Teukolsky, Nature (London) **238**, 211 (1972).
[74] T. Damour and R. Ruffini, Phys. Rev. D **14**, 332 (1976).
[75] T. Damour and M. Lilley, arXiv:0802.4169v1.